

Lawrence Berkeley National Laboratory

Lawrence Berkeley National Laboratory

Title

Numerical modeling of water injection into vapor-dominated geothermal reservoirs

Permalink

<https://escholarship.org/uc/item/06p9z28w>

Author

Pruess, Karsten

Publication Date

2008-06-20

NUMERICAL MODELING OF WATER INJECTION INTO VAPOR-DOMINATED GEOHERMAL RESERVOIRS

Karsten Pruess

Earth Sciences Division, Lawrence Berkeley National Laboratory
Berkeley, CA 94720

K_Pruess@lbl.gov

Abstract

Water injection has been recognized as a powerful technique for enhancing energy recovery from vapor-dominated geothermal systems such as The Geysers. In addition to increasing reservoir pressures, production well flow rates, and long-term sustainability of steam production, injection has also been shown to reduce concentrations of non-condensable gases (NCGs) in produced steam. The latter effect improves energy conversion efficiency and reduces corrosion problems in wellbores and surface lines.

This report reviews thermodynamic and hydrogeologic conditions and mechanisms that play an important role in reservoir response to water injection. An existing general-purpose reservoir simulator has been enhanced to allow modeling of injection effects in heterogeneous fractured reservoirs in three dimensions, including effects of non-condensable gases of different solubility. Illustrative applications demonstrate fluid flow and heat transfer mechanisms that are considered crucial for developing approaches to *in situ* abatement of NCGs.

Introduction

Vapor-dominated geothermal reservoirs such as The Geysers, California, are by their very nature water-short systems. Connate waters provide an inventory of heat transmission fluid that is insufficient for extracting more than a fraction of stored heat. Large-scale production at The Geysers with inadequate fluid replacement by injection led to strong declines in reservoir pressures and well flow rates during the 1980s and early 1990s (Sanyal et al., 2000). The installed electric generating capacity peaked around 1990 at about 2,000 MW and subsequently declined. A systematic program of increasing injection has been implemented, that uses condensate from the cooling towers, local creek water, and recycled waste water from neighboring communities that is sent by pipeline to The Geysers. The SEGEP pipeline from Lake and Sonoma counties is capable of delivering up to 36,000 metric tons of water per day (Smith et al., 2000). The Santa Rosa Geysers Recharge Project (SRGRP) provides as much as 42,000 metric tons of tertiary-treated municipal wastewater via a 65-km pipeline from Santa Rosa (Stark et al., 2005). Injection has been shown to provide pressure support to the reservoir, and in addition has substantially benefited energy extraction by reducing the amount of non-condensable gases (NCGs) in produced steam (Stark and Koenig, 2001).

Water injection is not automatically beneficial, however. In some cases injection has caused enthalpy declines at offset production wells, due to preferential migration of injected waters along major fractures that provided insufficient opportunity for heat transfer and fluid dispersal. A detailed understanding of the various physical and chemical processes induced by water injection into vapor-dominated reservoirs is needed in order to manage injection in a way that is most beneficial to energy extraction.

The physical processes induced by water injection into depleted or depleting vapor zones are characterized by a complex interplay between fluid flow and heat transfer, accompanied by phase change as injected water boils into steam. Additional complexities arise from the “dual porosity” nature of The Geysers reservoir, in which large-scale permeability is provided by networks of connected fractures, while matrix rocks of low permeability play an essential role as heat source to the injected fluid, as well as exchanging fluids with the fractures.

A number of studies published in the literature have demonstrated numerical simulation approaches for treating multi-phase fluids in dual-porosity systems, and for handling the extremely non-linear coupled fluid flow and heat transfer processes during production from and injection into vapor-dominated systems (Wu et al., 2004). However, mathematical modeling of injection into vapor-dominated systems remains a difficult task. Issues requiring additional research include (1) the interplay of multiple spatial scales for fluid migration along fractures and between fractures and matrix rocks, (2) vapor adsorption and capillary condensation effects, (3) numerical artifacts arising from finite spatial resolution of gradients in temperature and fluid saturation, (4) behavior of strongly water-soluble gases, such as HCl and NH₃, during fluid injection and production, and (5) chemical and mechanical interactions between reservoir fluids and rocks.

The present report is part of a study that is focused on the coupled fluid flow, heat transfer, and geochemical effects induced by large-scale injection into vapor-dominated system. Our primary interest is in gas-rich and depleted vapor zones, and the mechanisms through which injection could improve not only well flow rates and energy extraction, but help reduce concentrations of corrosive non-condensable gases such as HCl and CO₂ in produced steam.

Theoretical Considerations

One possible way to reduce HCl and other NCGs in Geysers steam would be to scrub them out *in situ*, by dissolving them in an aqueous phase that would be introduced by means of appropriately placed water injection. Although conceptually simple, a “literal” implementation of this idea seems unworkable, because in practice it would not be possible to control where the injected liquid goes, so that the idea of placing water in the path of steam flowing to the production wells seems unrealistic. However, it may be possible to achieve removal of NCGs *in situ* even if no specific control can be exerted on the migration of injected water. Injected water will be heated by contact with the reservoir rocks and will begin to vaporize when its temperature reaches the saturation temperature at prevailing reservoir pressures. The vaporization will cause volume expansion and pressurization that will propagate fairly rapidly outward, away from the injection plume. Liquid saturations will then increase throughout the volume in which steam pressures rise, by a combination of vapor adsorption on mineral surfaces

and condensation effects in small capillaries (Pruess and O’Sullivan, 1992). This well-known phenomenon is quantitatively described by Kelvin’s equation, which expresses vapor pressure as a function of temperature and liquid saturation,

$$P_{\text{vap}}(T, S_{\text{liq}}) = f_{\text{VPL}}(T, S_{\text{liq}}) \cdot P_{\text{sat}}(T) \quad (1)$$

Here

$$f_{\text{VPL}} = \exp\left[\frac{M_w P_{\text{suc}}(S_{\text{liq}})}{\rho_{\text{liq}} R (T + 273.15)}\right] \quad (2)$$

is the vapor pressure lowering (VPL) factor. P_{sat} is the saturated vapor pressure of bulk aqueous phase, the “suction pressure” $P_{\text{suc}} < 0$ is the difference between aqueous and gas phase pressures, ρ_{liq} is liquid density, M_w is the molecular weight of water, R is the universal gas constant, and T is temperature in °C. “Suction pressure” P_{suc} is a phenomenological concept that includes conventional capillary pressures, as well as pressures generated by adsorption of liquid water on hydrophilic mineral surfaces. When the ratio $P_{\text{vap}}/P_{\text{sat}}$ increases due to pressurization from injection-derived steam (IDS), we have $f_{\text{VPL}} \implies 1$ from Eq. (1), and $P_{\text{suc}} \implies 0$ from Eq. (2), to which corresponds an increasing amount of condensed phase S_{liq} .

As vapor pressures rise throughout a broad zone surrounding the injection plume, the additional condensed (liquid) phase formed can dissolve NCGs according to Henry’s law.

$$P_{\text{NCG}} = K_H \cdot x_{\text{NCG}} \quad (3)$$

Here, P_{NCG} is the partial pressure of the NCG, K_H is Henry’s coefficient (units of Pascals), and x_{NCG} is the mole fraction of NCG dissolved in the liquid phase. Henry’s coefficient describes partitioning of a volatile and water-soluble compound between two phases and can be regarded as an inverse solubility. It is a function of temperature and also depends on the composition and state of tension (suction pressure) of the condensed aqueous phase. Typical values of Henry’s

coefficient for pure water (no salinity) are of order 10^{10} Pa for a sparingly soluble gas such as nitrogen, 5×10^8 Pa for CO_2 , and 10^5 Pa or less for highly soluble HCl.

The propagation of vapor pressure increases outward from the injection plume is described by a parabolic (diffusive) equation, suggesting that it may be possible to increase condensed phase saturations broadly, throughout a large region. Such condensed phase may be effective in dissolving highly soluble corrosive gases such as HCl. To achieve this effect it will not be necessary to place the actual injection water into the pathway of the steam towards the production wells. Once the HCl is dissolved, additional beneficial effects may be derived from chemical interactions with rock minerals that would buffer the acidity.

Test Problems

Numerical simulations of water injection and steam production were performed using an idealized five-spot well configuration as shown in Figure 1. The same setup had been employed in previous studies of reservoir processes at The Geysers, and similar reservoir parameters were used here as in earlier studies (Pruess, 2002). A five-spot configuration is commonly used for studies of geothermal production and injection, even though in reality injection and production wells will rarely if ever be arranged in such a regular pattern (Sanyal and Butler, 2005). The geometric idealization of the five-spot configuration has a high degree of symmetry, allowing to

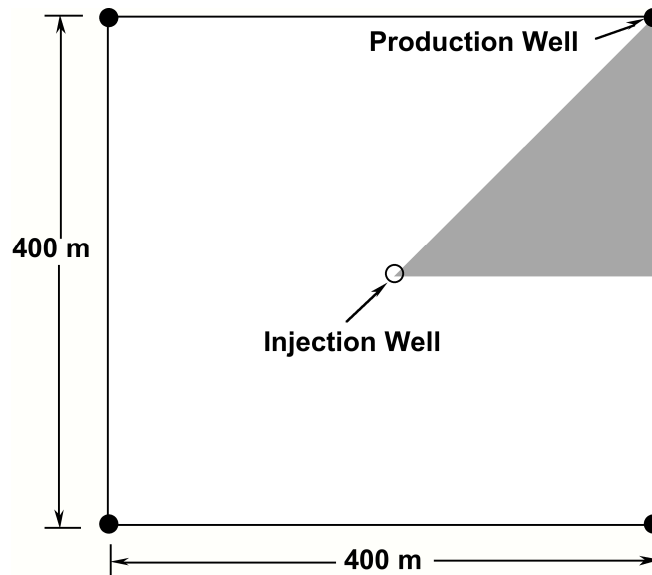


Figure 1. Schematic of five-spot production-injection system, with shading showing a 1/8 symmetry element.

work with a reservoir subdomain of limited spatial extent, so that reasonable spatial resolution can be achieved without requiring an inordinately large numbers of grid blocks. Because of symmetry, only 1/8 of the basic five-spot pattern needs to be modeled, and a 5-point parallel grid (Pruess, 1991) of 196 square blocks with 10.88 m length was used to represent one layer of this 1/8 symmetry element. Reservoir thickness was 500 m, which for our 3-D simulations was divided into five layers of 100 m thickness each. Some simulations used a single porous medium description for the reservoir, while others employed a fractured reservoir description, using the method of “multiple interacting continua” (MINC; Pruess and Narasimhan, 1985; see Fig. 2).

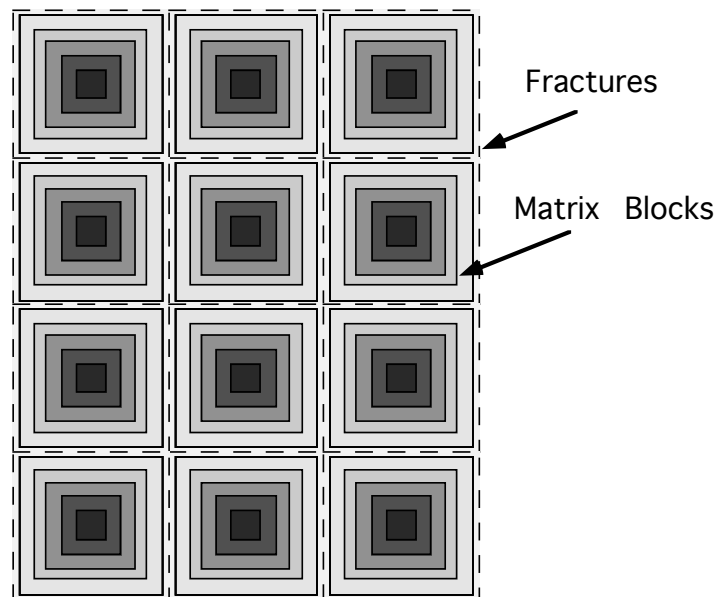


Figure 2. Subgridding in the method of “multiple interacting continua” (MINC), showing rock matrix blocks of low permeability separated by a network of fractures.

Our five-layer 3-D porous medium model has a total of $5 \times 196 = 980$ grid blocks. In the MINC model, each of the porous medium blocks is subdivided into one fracture and four rock matrix blocks, for a total of $5 \times 980 = 4,900$ blocks. Table 1 lists reference parameters used for a 3-D single-porosity model, in which constant conditions of $(T, P) = (250 \text{ }^\circ\text{C}, 30 \text{ bar})$ are employed at the lower boundary to represent a depleted reservoir zone that is fed by steam rising from depth. Additional parameters used for the fractured reservoir problem are given in Table 2. Production is specified by maintaining constant pressure conditions in the production grid blocks (top three

Table 1. Specifications of five-spot single-porosity reservoir problem

Reservoir properties		
Horizontal permeability		$43.2 \times 10^{-15} \text{ m}^2$
Porosity		4 %
Thickness		500 m
Vertical permeability		$43.2 \times 10^{-15} \text{ m}^2$ (top 300 m) $10 \times 10^{-15} \text{ m}^2$ (bottom 200 m)
Relative permeability liquid: van Genuchten (1980); parameters gas: Corey (1954); parameter		$\lambda = 0.4438$; $S_{lr} = 0.80$ $S_{gr} = 0.05$
Capillary pressure van Genuchten (1980); parameters		$\lambda = 0.4438$; $S_{lr} = 0$; $P_0 = 17.27 \times 10^5 \text{ Pa}$
Pattern area		$160,000 \text{ m}^2$ (= 39.5 acres)
Well spacing (distance from injector to producer)		282.8 m (928.0 ft)
Initial production rate (full well basis)		10.45 kg/s
Injection [#] rate (full well basis) ^{&} enthalpy		40 kg/s 100 kJ/kg
Gridding horizontal: 5-point parallel grid, spacing vertical: 5 layers, thickness		10.88 m 100 m
Boundary conditions	top bottom	no flow $T = 250 \text{ }^\circ\text{C}$, $P = 30 \text{ bar}$
Initial conditions		steady state (see text)

[#] injection well is assumed open in the top layer only.

[&] “full well basis” means rate for the entire well, which is 8 times the value used in the 1/8 symmetry domain considered in our model.

layers). For the 10.88 m grid spacing used here this corresponds to an effective wellbore radius of 6.14 m, or a skin factor of -4.1 for an 8’’ well ($r_w = 4’’ = 10.16 \text{ cm}$), a value that is not unreasonable for wells at The Geysers. Flowing bottomhole pressure is specified as 8 bar opposite the top layer of the model. Initial conditions for this case are prepared by running the system to steady state, resulting in a production rate of 6.56 kg/s (full well basis) and conditions of $(T, P) \approx (225 \text{ }^\circ\text{C}, 15 \text{ bar})$ in the top layer, with a liquid saturation of $S_l \approx 4 \%$. Injection is then made at a rate of 40 kg/s (full well basis). The possibility that liquid water may be trapped in the tight matrix rock is accounted for in the porous medium model by specifying a large irreducible water saturation of 80 %. Some variations of the reference parameters were explored, as was

behavior of non-condensable gases with a range of solubilities in the aqueous phase (see “Results” section, below). All simulations reported here were made with our general-purpose reservoir simulator TOUGH2 and the EOS4 fluid property module for water-NCG mixtures including VPL effects (Pruess et al., 1999; Pruess, 2004). Special enhancements were implemented to allow modeling of NCGs with different molecular weight and aqueous solubility. An existing grid generator for 3-D five-spot grids was extended to be able to interface with the MINC subgridding process required for fractured media, and various enhancements were made for generating output data of interest in the context of *in situ* NCG abatement in vapor-dominated systems.

Table 2. Additional specifications for the fractured reservoir problem

Reservoir properties		
Average permeability (of fracture network)		$43.2 \times 10^{-15} \text{ m}^2$
Matrix permeability		$1.9 \times 10^{-18} \text{ m}^2$
Klinkenberg parameter		$7.6 \times 10^5 \text{ Pa}$
Fracture porosity	average	1 %
	intrinsic	50 %
Matrix porosity		3 %
Thickness		500 m
Relative permeability liquid: van Genuchten (1980); parameters gas: Corey (1954); parameter		$\lambda = 0.4438$; $S_{lr} = 0.08$ $S_{gr} = 0.05$
Capillary pressure van Genuchten (1980); parameters		$\lambda = 0.4438$; $S_{lr} = 0$; $P_0 = 3238 \text{ Pa}$ (fractures); $17.27 \times 10^5 \text{ Pa}$ (matrix)
MINC subgridding number of continua volume fractions		5 0.02, 0.08, 0.20, 0.35, 0.45
Diffusion parameters for NCG molecular weight gas phase diffusivity ^{&} aqueous diffusivity tortuosity in fractures tortuosity in matrix		36.45 (HCl) $1.7 \times 10^{-5} \text{ m}^2/\text{s}$ $1.7 \times 10^{-9} \text{ m}^2/\text{s}$ 1.0 0.01

[&] at standard conditions of $P_0 = 1 \text{ atm}$, $T_0 = 0 \text{ }^\circ\text{C}$

Results

Single-Porosity Reservoir Problem

As the injected water migrates outward, away from the injection point, it is being heated and partially vaporized by contact with the reservoir rocks. Fig. 3 shows the complex non-monotonic behavior of fluid pressures resulting from injection. Along a line from the injection to the production point (going from right to left in Fig. 3), there initially is a strong pressure decline. Then a local minimum is reached, followed by pressure increase and a local maximum, and subsequently there is a gradual decline towards the production well. Over time this pattern persists and moves towards larger distance from the injector.

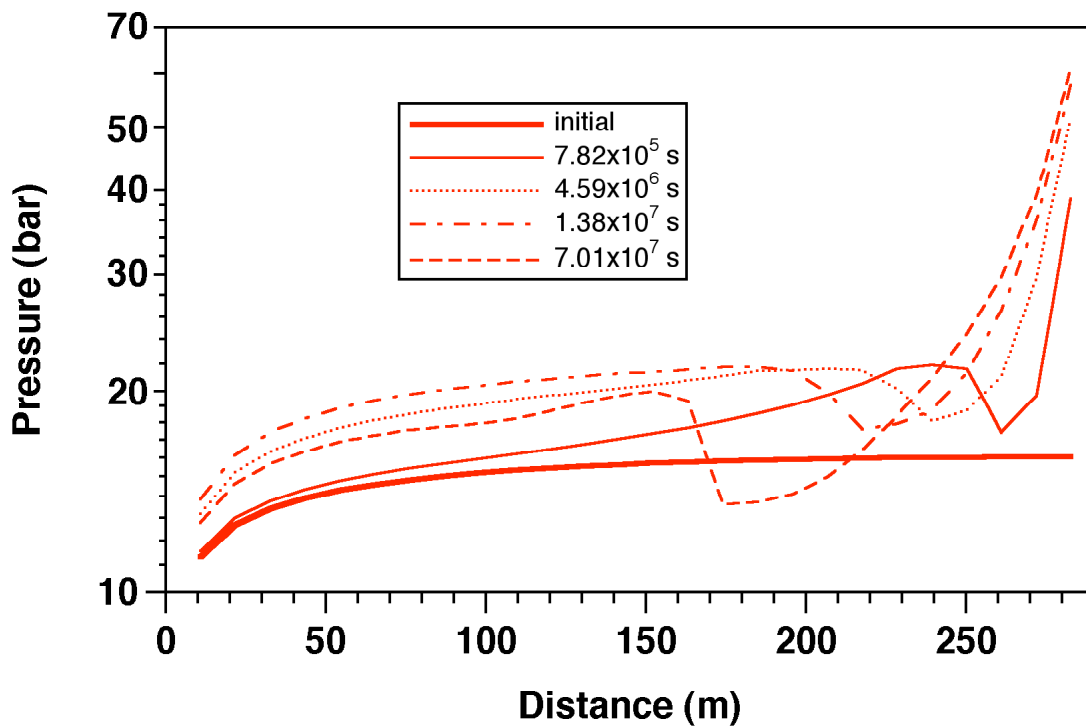


Figure 3. Pressure profiles at different times in the top reservoir layer along a line extending from the production well (at distance 0) to the injection well (located at a distance of 282.8 m).

The pressure behavior arises from an interplay of single-phase liquid flow near the injection well with two-phase steam-water flow under non-isothermal conditions at larger distance. In the region with steep pressure gradients around the injector we have single-phase

liquid. Pressure gradients increase in this region over time, due to strong increases in water viscosity as temperatures decline from continued injection. The local minimum in pressure occurs at the outer boundary of the single-phase liquid region (compare water saturations in Fig. 4). At larger distance from the injector two-phase water-steam conditions are present. The inner

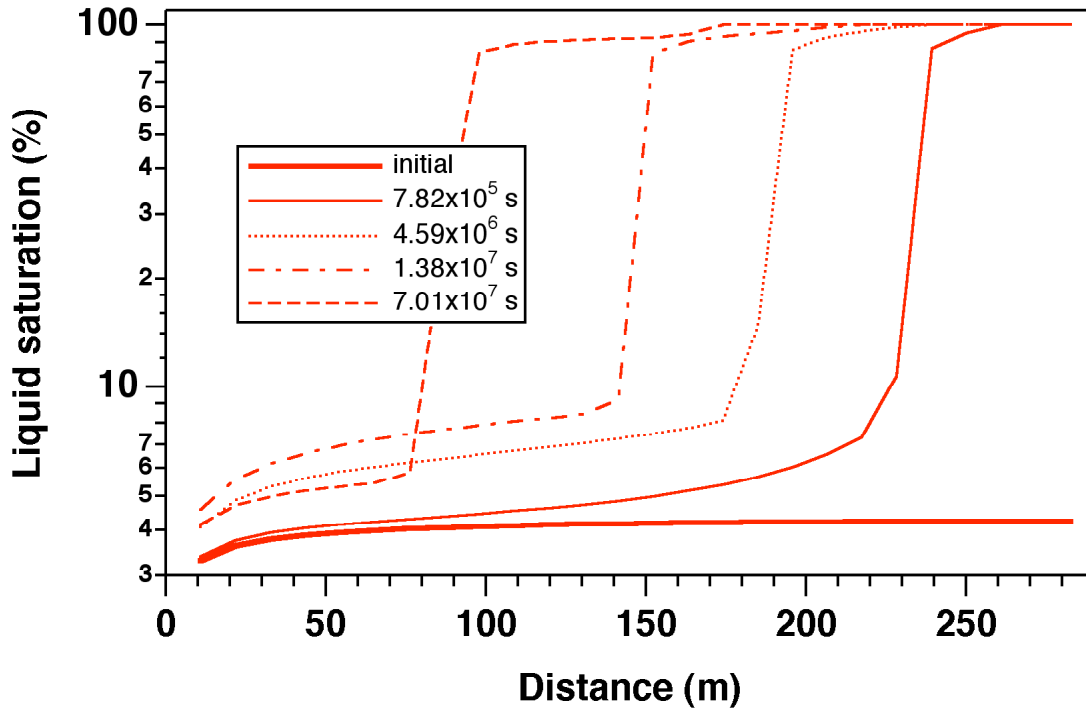


Figure 4. Liquid saturation profiles at different times in the top reservoir layer along a line extending from the production well (at distance 0) to the injection well (located at a distance of 282.8 m)..

portion of the two-phase zone is cooled by injected water. The cooling is most pronounced closest to the injection plume, and becomes weaker at increasing distance from the injection well. Thus, the lowest temperature in the two-phase zone occurs at its inner boundary, while temperatures increase at larger distance from the injection well. Due to the coupling between temperatures and pressures in two-phase conditions (Eq. 1), the temperature increase going outward in the two-phase zone causes vapor pressures to increase as well. Water saturations generally decrease with increasing distance from the injection point (Fig. 4). At larger distance

from the injection point, associated vapor pressure lowering effects (declining f_{VPL} coefficient in Eq. 2 as water saturation decreases) become stronger than increases in saturated vapor pressure due to increasing temperatures, giving rise to a local maximum in vapor pressure. Beyond the local pressure maximum there is a monotonic pressure gradient towards the production well. In the region between the local maximum and local minimum in pressure, steam flows towards rather than away from the injection point. Liquid phase pressures decline monotonically away from the injection point, due to capillary pressure gradients that are stronger than the increases in steam pressure. Thus, liquid water flows away from the injection point everywhere. In the inner (near-injector) portion of the two-phase zone, we therefore have a steam-water counterflow, with water flowing away from and steam flowing towards the injection point. The steam flowing towards the liquid portion of the injection plume condenses there, depositing its latent heat of vaporization and heating injected water.

Pressures near the injection well continue to increase over time, but it is interesting to note that at late time pressures in the more distant portions of the two-phase zone actually decline. This is a consequence of overall temperature decline due to heat transfer from the rock to injected water. As had been anticipated, increases in water saturation occur far ahead of the actual injection plume (Fig. 4), due to partial condensation of steam caused by increasing vapor pressures.

At early time, only a small fraction of the injected liquid is vaporized (Fig. 5), which can be understood from the small geometric size of the injection plume. Only a small reservoir volume is contacted by the injected water, and steam is generated in a small radius around the injection well. Steam fluxes are limited by limited surface area of the injection plume, and the large pressure gradients required to allow steam to flow outward. Over time the injection plume grows outward and eventually downward as well. This facilitates heat transfer and steam flow away from the surface of the plume, causing an increasing fraction of injectate to be vaporized. Our simulation ends after 400 time steps at a time of 70.1×10^6 s (115.9 weeks), at which time more than 40 % of total injected liquid has been vaporized.

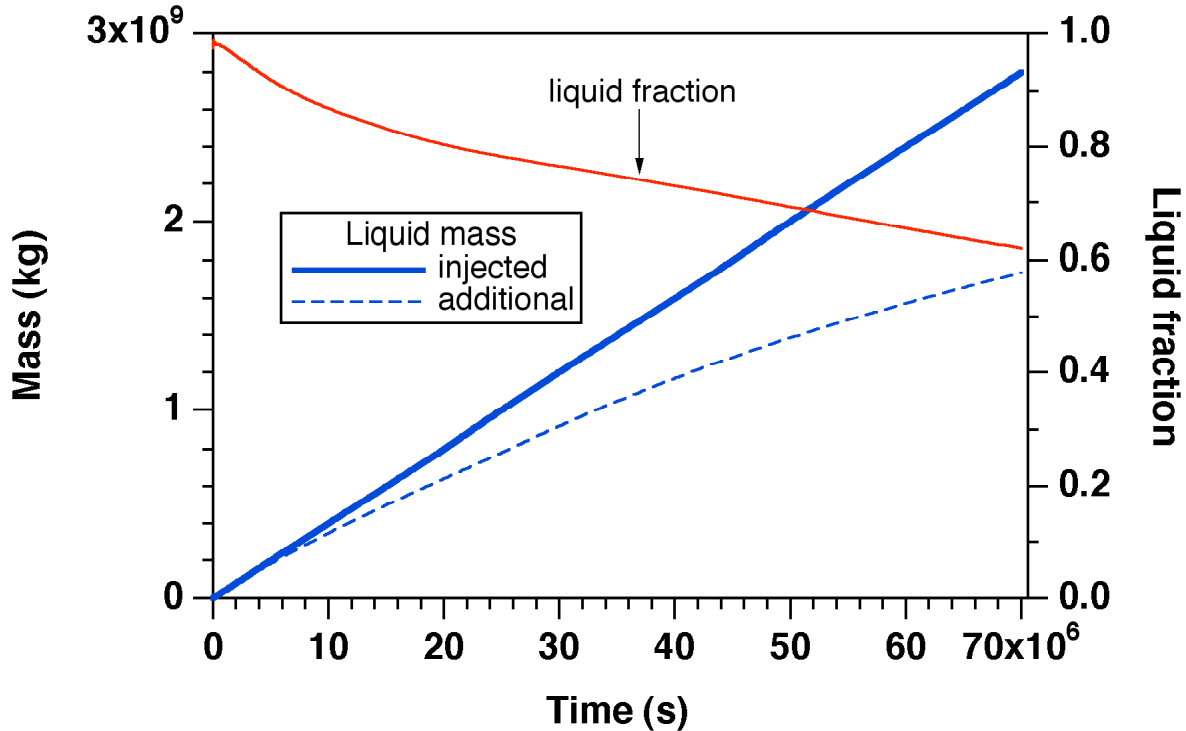


Figure 5. Mass balance for liquid phase on a full-well basis. For the applied constant injection rate of 40 kg/s, the mass of injected liquid grows linearly with time. The dashed curve (labeled “additional”) shows the increase in liquid mass in the reservoir with time. The difference between “injected” and “additional” liquid mass indicates the amount of liquid that is vaporized. The fraction of injected liquid remaining as liquid in the reservoir (unvaporized) is also shown.

The steam production rate shows a non-monotonic behavior, more than doubling over the first 20×10^6 s, and then slowly declining (Fig. 6). The decline is due to a slow decrease in temperature over the surface of the expanding injection plume and associated pressure decrease. Fig. 6 also shows NCG mass fractions in produced steam, for three different values of NCG solubility (Henry’s coefficient). For modeling NCG behavior, the initial (pre-injection) steady state was prepared by specifying a small, constant NCG partial pressure at the bottom boundary, typically in the range of 10 – 1000 Pa. Steam flow rates are not affected by the presence of small concentrations of NCG. For the lower-solubility gases ($K_H = 10^{10}$ and 10^7 Pa), injection gives rise to a brief increase in NCG concentration, followed by a step decline. This behavior can be seen more clearly in the early-time plot, Fig. 7. For a high-solubility NCG ($K_H = 10^5$ Pa) the decline is monotonic but weaker, and long-term NCG concentrations remain much higher. These

outcomes can be readily understood as follows. For NCGs with low aqueous solubility (large K_H), the partial steam condensation induced by injection-derived pressurization (Fig. 3) will leave the residual steam enriched in NCGs and will increase NCG concentrations in produced steam. Such increase is temporary, however, because over time an increasing fraction of produced steam is derived from vaporization of injected water, which is low in NCGs. For NCGs with large solubility, pressurization-induced condensation will cause substantial dissolution of NCGs, and will reduce NCG concentrations in residual steam. Long-term NCG concentrations in produced steam remain higher for more soluble NCGs, however, because there is a larger inventory dissolved in the condensed phase that continues to supply NCGs to the steam through slow evaporation.

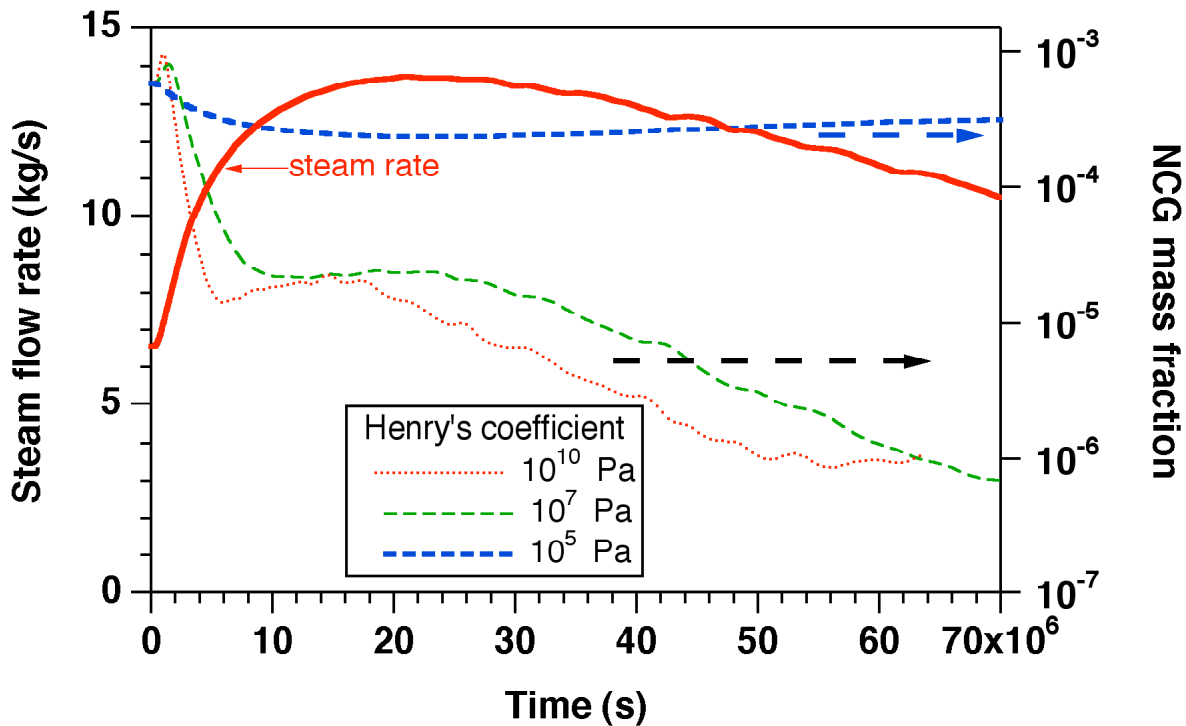


Figure 6. Steam production rate (full-well basis) and NCG mass fractions in produced steam for NCGs with different solubilities. (Henry's coefficient is inverse solubility.)

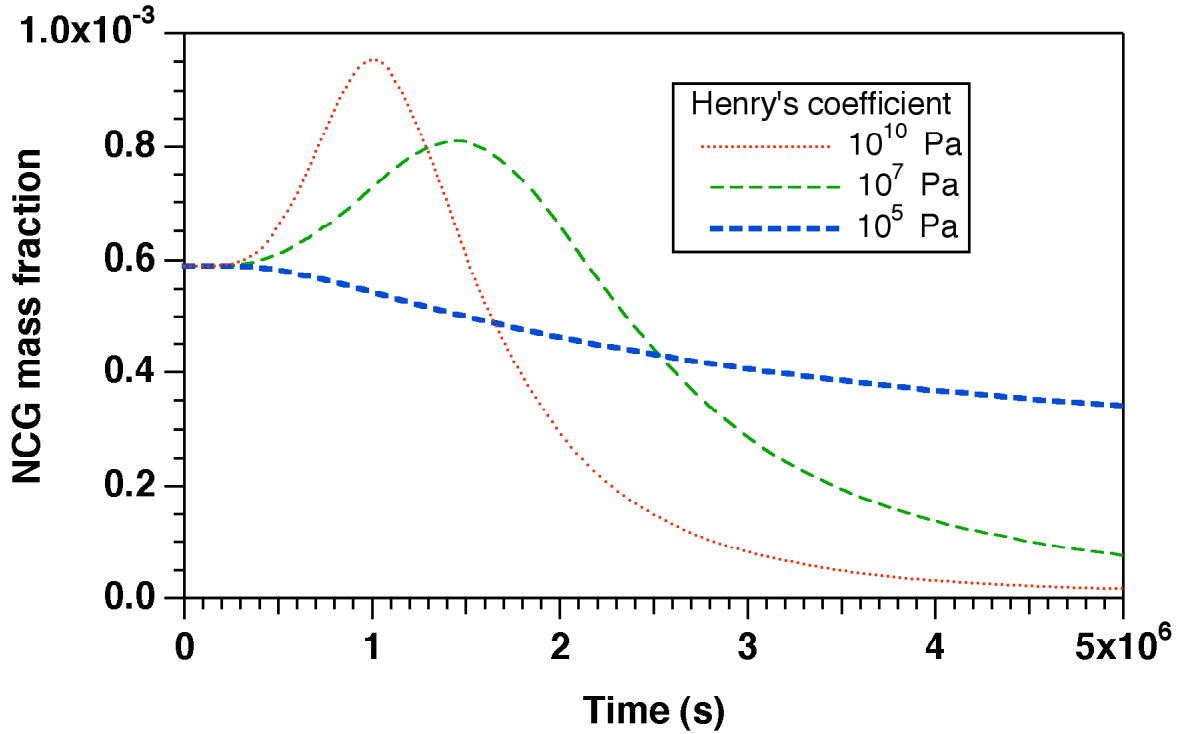


Figure 7. NCG mass fractions in produced steam at early times for NCGs with different solubilities. (Henry's coefficient is inverse solubility.)

3-D Fractured Reservoir Problem

The numerical simulation of the fractured reservoir system is considerably more difficult than for the porous medium, for the following reasons: (1) the total number of grid blocks is increased by a factor 5; (2) the fracture grid blocks have small volumes, which limits time step sizes; (3) the fracture-matrix interaction is extremely non-linear, due to very strong capillary pressures in the rock matrix; (4) in addition to advective effects, NCG behavior is strongly influenced by molecular diffusion between fractures and rock matrix. The numerical simulations presented here are the first quantitative analyses of water injection into a fully 3-D fractured reservoir system with inclusion of NCG effects. Results for a time period of 37.7×10^6 s (436.6 days) are shown in Figs. 8 and 9.

Prior to startup of injection, all of the liquid present in the system resides in the rock matrix. This is because suction pressure and VPL effects are very weak in the fractures, so that at

pressures substantially below saturated vapor pressure no condensed phase can be formed in the fracture domain. In response to water injection, liquid mass increases in both fractures and rock matrix, the latter being due to (capillary) suction effects that draw liquid from the fractures into the rock matrix (Fig. 8). For an initial period of approximately 8×10^6 s, most of the increase in liquid mass in the reservoir occurs in the fracture system. At later time, the increase in liquid inventory of the fractures tapers off, and most increase occurs in the rock matrix. Comparing

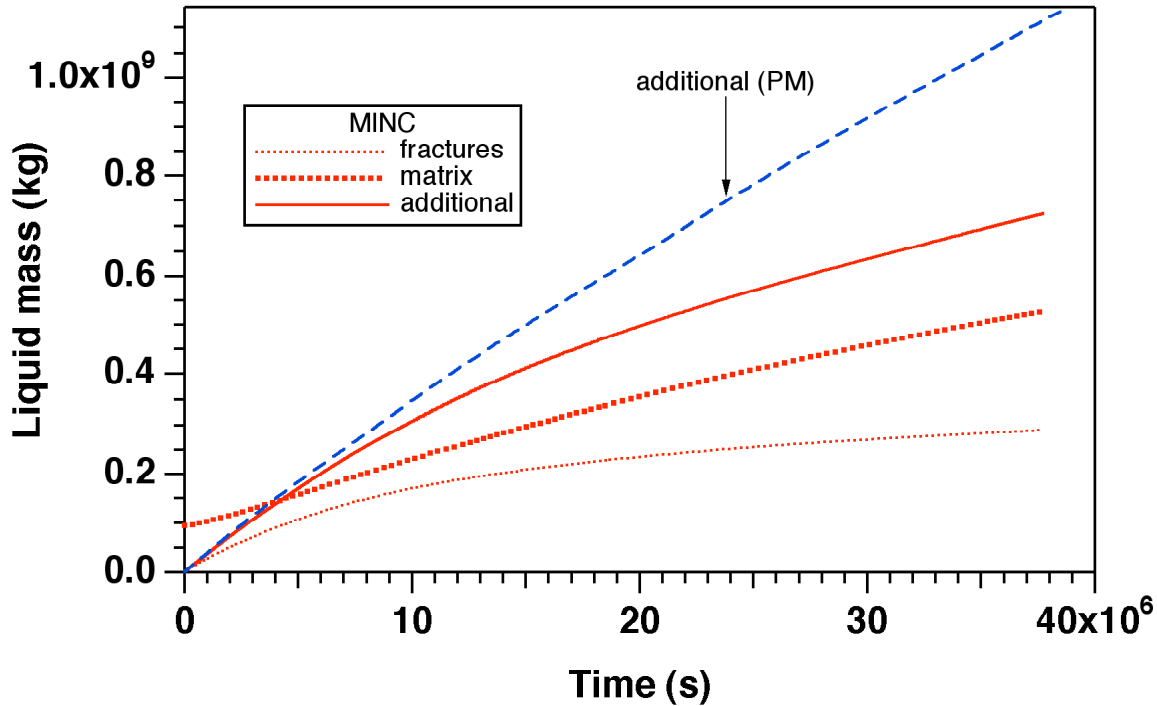


Figure 8. Liquid mass balances for the 3-D fractured reservoir system (MINC; full-well basis). Total additional liquid mass (injected liquid that remains unvaporized) calculated for the porous medium (PM) model is also shown.

with the porous medium model (Fig. 5), Fig. 8 shows that increase of liquid mass in the fracture system is significantly smaller. Fig. 9 shows that steam production in the fractured reservoir responds more rapidly to injection than was the case for the porous medium model. This is because pressurization effects from injection propagate more rapidly in the fracture system, due to its smaller pore volume. The longer-term increase in steam production induced by injection is smaller, however, than for the porous medium, and decline from the local maximum sets in

earlier and is steeper than in the porous medium case. These latter effects are primarily due to heat transfer limitations in the fractured medium. In the porous medium model, heat transfer from rocks to fluids is local and instantaneous, while in the fractured reservoir description, heat transfer occurs by conduction from the interior of low-permeability matrix blocks to the surrounding fracture network. Conduction is a slow process, so that rates of heat transfer to the injection plume, hence vaporization rates, are smaller.

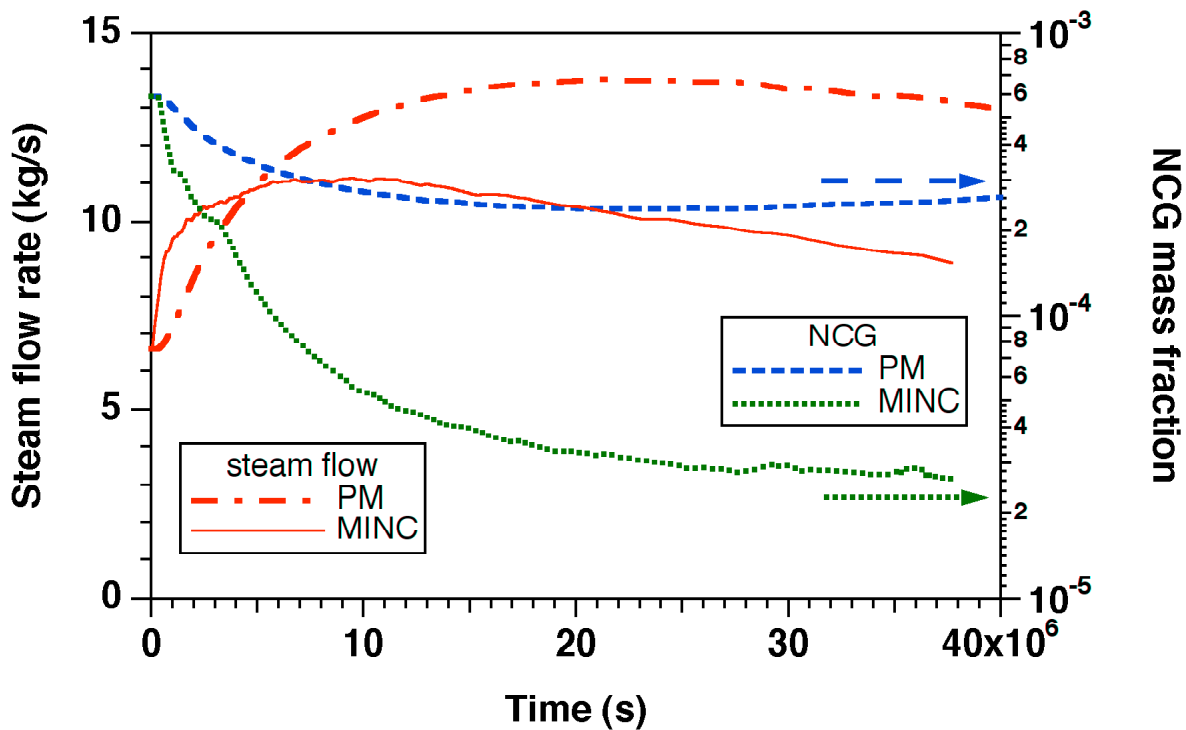


Figure 9. Comparison of steam flow rates (full-well basis) and NCG concentrations in produced steam for the fractured (MINC) and porous medium (PM) models. The NCG calculation is for a highly soluble gas with a Henry's coefficient of $K_H = 10^5$ Pa.

From the steam production rates shown in Fig. 9 it is evident that long-term cumulative steam production is smaller in the fractured (MINC) than in the porous medium model. Fig. 8 shows that cumulative addition of liquid phase to the fractured reservoir is also smaller. Given that rates of fluid injection are the same in both systems, this raises a question as to overall mass conservation in the fractured reservoir. Inspecting our simulation results, the simple answer to

this seeming inconsistency is that the “missing” portion of the injected fluid leaves the fractured reservoir through the lower boundary of the system, at 500 m depth below the reservoir top, and is then no longer included in the mass balances for the top 500 m of reservoir that is considered in our model. There is a point of practical importance here, namely, that due to the relatively small volume of the fracture system (here assumed as 1 % of total reservoir volume), and due to heat transfer limitations in a fractured reservoir, a substantial fraction of injected liquid migrates fairly rapidly to considerable depth. Vertical downflow of unvaporized liquid water is a much smaller effect in the porous medium model.

Fig. 9 shows that NCG concentrations in produced steam decline much more rapidly in the fractured reservoir than in the porous medium. This is due to two effects, (1) NCG-rich steam is rapidly purged from the fracture system by vaporization of injectate, and (2) most of the NCG inventory of the fractured reservoir is in the rock matrix, from where it can reach the fracture system only by molecular diffusion, which is a slow process.

Concluding Remarks

The studies presented here have demonstrated numerical simulation capabilities for accurate modeling of the thermodynamics of NCG-water mixtures under non-isothermal multiphase conditions in porous media. Flow and transport processes in three dimensions can be modeled taking into account heterogeneous hydrogeologic properties, including fracture networks, and fracture-matrix interaction due to diffusion, advection, and heat conduction. Future work will consider chemical reactions between aqueous fluids and reservoir rocks as well.

Our simulations have shown significant vapor pressure increases from injection, condensation effects arising from the pressurization, and NCG dissolution effects in the condensed phase. These effects form possible building blocks for achieving *in situ* abatement of NCGs, which is the central objective of the present project. Future studies will investigate possibilities and limitations for using targeted water injection to control NCGs, and to aid in design and interpretation of laboratory experiments that are currently being assembled.

Acknowledgement

Thanks are due to Tim Kneafsey and Nic Spycher for a careful review of the manuscript and suggestions for improvements. This work was supported by a PIER grant from the California Energy Commission (CEC) and by the Assistant Secretary for Energy Efficiency and Renewable Energy, Office of Geothermal Technologies, of the U.S. Department of Energy under Contract No. DE-AC02-05CH11231.

References

- Pruess, K. Grid Orientation and Capillary Pressure Effects in the Simulation of Water Injection into Depleted Vapor Zones, *Geothermics*, Vol. 20, No. 5/6, pp. 257 - 277, 1991.
- Pruess, K. Numerical Simulation of Multiphase Tracer Transport in Fractured Geothermal Reservoirs, *Geothermics*, Vol. 31, pp. 475 - 499, 2002.
- Pruess, K. The TOUGH Codes—A Family of Simulation Tools for Multiphase Flow and Transport Processes in Permeable Media, *Vadose Zone J.*, Vol. 3, pp. 738 - 746, 2004.
- Pruess, K., C. Oldenburg and G. Moridis. TOUGH2 User's Guide, Version 2.0, Lawrence Berkeley National Laboratory Report LBNL-43134, Berkeley, CA, November 1999.
- Pruess, K. and M. O'Sullivan. Effects of Capillarity and Vapor Adsorption in the Depletion of Vapor-Dominated Geothermal Reservoirs, Lawrence Berkeley Laboratory Report LBL-31692, presented at Seventeenth Workshop on Geothermal Reservoir Engineering, Stanford University, Stanford, CA, January 1992.
- Pruess, K. and T.N. Narasimhan. A Practical Method for Modeling Fluid and Heat Flow in Fractured Porous Media, *Soc. Pet. Eng. J.*, 25 (1), 14-26, February 1985.
- Sanyal, S.K. and S.J. Butler. An Analysis of Power Generation Prospects from Enhanced Geothermal Systems, *Proceedings, Paper 1632.pdf*, World Geothermal Congress 2005, Antalya, Turkey, 24-29 April 2005.

- Sanyal, S.K., S.J. Butler, P.J. Brown, K. Goyal, and T. Box. An Investigation of Productivity and Pressure Decline Trends in Geothermal Steam Reservoirs, *Proceedings, World Geothermal Congress 2000*, pp. 873 - 877, International Geothermal Association, May-June 2000.
- Smith, B., J. Beall and M. Stark. Induced Seismicity in the SE Geysers Field, California, USA, *Proceedings, World Geothermal Congress 2000*, pp. 2887 - 2892, International Geothermal Association, May-June, 2000.
- Stark, M. and B. Koenig. Generation Gain in the Northern Geysers Due to Injection-Derived NCG Reduction, *Transactions, Geothermal Resources Council*, Vol. 25, pp. 469-474, 2001.
- Stark, M.A., W.T. Box Jr., J.J. Beall, K.P. Goyal, and A.S. Pingol, The Santa Rosa – Geysers Recharge Project, Geysers Geothermal Field, California, USA, *Proc. World Geotherm. Cong. 2005*, paper 2420, 2005.
- Wu, Y.S., L. Pan and K. Pruess. A Physically Based Approach for Modeling Multiphase Fracture-Matrix Interaction in Fractured Porous Media, *Advances in Water Resources*, Vol. 27, pp. 875 - 887, 2004.